



**HAL**  
open science

## Low temperature study of phase equilibria in the Co–Ni–W ternary system: Evidence of a new intermetallic phase Co<sub>3</sub>W-D0a

Nicolas Bouliez, Jérôme Andrieux, Rodica Chiriac, François Toche,  
Jean-Claude Crivello, Bruno Gardiola, Sophie Cazottes, Florence Robaut,  
Rafael Cury, Olivier Dezellus

### ► To cite this version:

Nicolas Bouliez, Jérôme Andrieux, Rodica Chiriac, François Toche, Jean-Claude Crivello, et al..  
Low temperature study of phase equilibria in the Co–Ni–W ternary system: Evidence of a  
new intermetallic phase Co<sub>3</sub>W-D0a. *Journal of Alloys and Compounds*, 2022, 892, pp.162109.  
10.1016/j.jallcom.2021.162109 . hal-03371636

**HAL Id: hal-03371636**

**<https://hal.science/hal-03371636>**

Submitted on 13 Oct 2022

**HAL** is a multi-disciplinary open access archive for the deposit and dissemination of scientific research documents, whether they are published or not. The documents may come from teaching and research institutions in France or abroad, or from public or private research centers.

L'archive ouverte pluridisciplinaire **HAL**, est destinée au dépôt et à la diffusion de documents scientifiques de niveau recherche, publiés ou non, émanant des établissements d'enseignement et de recherche français ou étrangers, des laboratoires publics ou privés.

# Low temperature study of phase equilibria in the Co–Ni–W ternary system: evidence of a new intermetallic phase

## $\text{Co}_3\text{W-}D0_a$

Nicolas Bouliez<sup>1,2</sup>, Jérôme Andrieux<sup>2</sup>, Rodica Chiriac<sup>2</sup>, François Toche<sup>2</sup>, Jean-Claude Crivello<sup>3</sup>, Bruno Gardiola<sup>2</sup>, Sophie Cazottes<sup>4</sup>, Florence Robaut<sup>5</sup>, Rafael Cury<sup>1</sup>, Olivier Dezellus<sup>2</sup>

<sup>1</sup> Plansee Tungsten Alloys, 446 avenue des Dignes, 74807 Saint Pierre en Faucigny, France

<sup>2</sup> Laboratoire des Multimatériaux et Interfaces, UMR CNRS 5615, Univ Lyon, Université Claude Bernard Lyon 1, F-69622 Villeurbanne, France.

<sup>3</sup> Univ Paris Est Creteil, CNRS, ICMPE, UMR7182, 2 rue Henri Dunant, 94320 Thiais, France.

<sup>4</sup> Université de Lyon, INSA Lyon, MATEIS, Bât. St Exupéry, 25 avenue Jean Capelle, Villeurbanne Cedex 69621, France.

<sup>5</sup> Univ. Grenoble Alpes, CNRS, Grenoble INP, SIMAP, F-38000 Grenoble, France

Corresponding author: [olivier.dezellus@univ-lyon1.fr](mailto:olivier.dezellus@univ-lyon1.fr)

---

### ABSTRACT

Tungsten heavy alloys (Co–Ni–W) of different compositions were prepared by powder metallurgy (solid sintering), heat treated at 800°C and 1000°C and subsequently analyzed. The experimental phase identifications and composition measurements emphasized discrepancies compared to the isothermal ternary sections simulated with commercial thermodynamic databases.

The isothermal sections at 800°C and 1000°C were found more complex than expected since a new intermetallic phase appeared to be stable ( $D0_a$  structure -  $\text{Cu}_3\text{Ti}$  prototype). Likewise, an interpretation of phase equilibria evolution with temperature was established to reach agreement with high temperature data. Formation enthalpies associated with the new phase were obtained through first-principles calculations and supported experimental results as they confirmed the stabilizing role of Ni addition for the  $D0_a$  structure.

---

### Keywords

**A. Intermetallics**

**B. Powder metallurgy**

**C. Phase diagrams**

**D. Thermal analysis; X-ray diffraction**

## 1. Introduction

The Co–Ni–W system is involved in many industrial applications including Co-based and Ni-based superalloys, cemented carbide materials or tungsten heavy alloys (WHAs). Ni-based superalloys are fit for turbojet engines and marine propulsion turbines. The alloying elements found in nickel based superalloys are chosen for solid solution and  $\gamma/\gamma'$  precipitation strengthening [1]. The nickel-based superalloys may comprise 10 alloying elements including Co and W and the resulting constitutional complexity must be controlled with care to avoid deleterious phase precipitation ( $\sigma$ ,  $\mu$ , and Laves phases) after long time operation at elevated temperatures [2]. WHAs are employed as balance weights, radiations shields and kinetic energy penetrators amongst other applications. Their W content may reach 96wt%. These alloys have a composite microstructure described by **Fig 1**. The hard tungsten nodules with a body-centered cubic lattice (called  $\alpha$  phase or BCC\_A2) are surrounded by a matrix which is a ternary solid solution with face-centered cubic lattice composed mostly of W, Ni, Co (called  $\gamma$  phase or FCC\_A1). The mechanical properties of WHAs are mainly driven by the interfacial strength between the  $\alpha$  and  $\gamma$  phases. Thus, it is of utmost importance to avoid intermetallic precipitation at interfaces during manufacturing processes as it causes severe embrittlement.

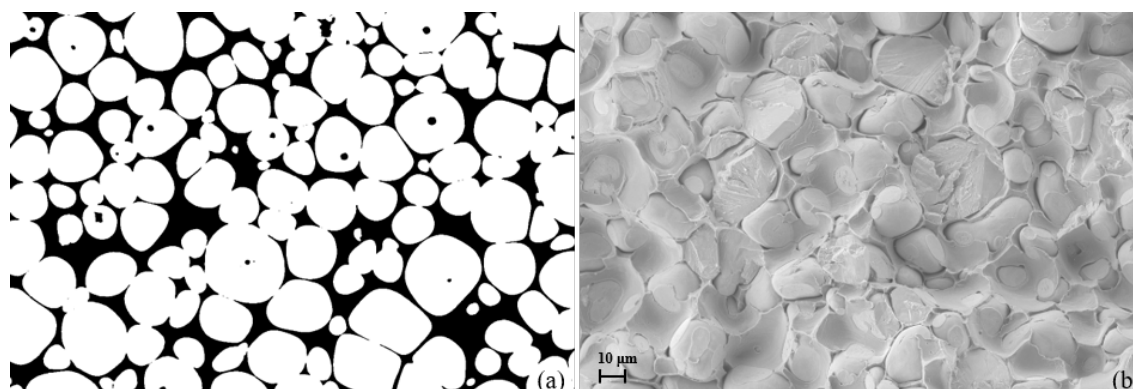


**Fig 1.** (a) WHAs composite microstructure (SEM/BSE) and (b) rupture analysis of an embrittled alloy (SEM/SE2) observed with magnification  $\times 500$ . - Source: Plansee Tungsten Alloys.

Nowadays alloy designs are computer assisted thanks to the CALPHAD method [3] which enables the assessment of phase equilibria and may predict the microstructure. However, CALPHAD modeling requires experimental data collected in the whole range of thermodynamic variables (mostly compositions and temperature). In the case of the Co–Ni–W system, several CALPHAD models were suggested for the binary subsystems Ni–W [4,5], Co–W [6–11] and Co–Ni [12], whereas only one attempt to model the ternary Co–Ni–W system is reported in the literature by Guillermet in 1988 [13]. At that time, few experimental results were available and most of them corresponded to high temperature phase equilibria at temperatures above 1300°C. Since then, new experimental results, obtained from diffusion multiples at intermediate temperatures (800 and 900°C), were reported [14] and are in contradiction with available thermodynamic description [13]. One of the most striking discrepancy is the Ni/Co substitution ratio in the  $\text{Co}_3\text{W}$  phase that is lower than 0.63 (29 at% Ni) according to Guillermet's model [13], while Zhu et al. [14] reported a maximum value of about 4 (62 at% Ni) at 800°C.

If confirmed, this extension of the  $\text{Co}_3\text{W-DO}_{19}$  phase might have important consequences, preventing for example the precipitation of  $\text{Co}_7\text{W}_6\text{-}\mu$  phase in FCC phase during heat treatment in this temperature range. Hence, new experimental data at intermediate temperatures are needed to improve the knowledge on phase stability in composition and temperature and phase equilibria in the ternary system. It is a mandatory step before any improvement of the CALPHAD model initially proposed by Guillermet.

In order to resolve this discrepancy concerning extension in composition of the  $\text{Co}_3\text{W-DO}_{19}$  phase below  $1000^\circ\text{C}$ , samples with different Ni/Co ratios and a constant tungsten content (30 at%) were synthesized and heat treated at  $800^\circ\text{C}$  and  $1000^\circ\text{C}$ . The samples were characterized by X-ray diffraction and electron diffraction, scanning electron microscopy, electron probe micro analysis and thermogravimetric - differential scanning calorimetric (TGA-DSC) analysis. Also, in order to sustain experimental results, formation enthalpies of intermetallic structures were obtained by electronic Density Functional Theory (DFT) calculations at 0 K.

## 2. Available thermodynamic descriptions

The Co–Ni binary system is characterized by a complete solid solubility in the FCC\_A1 phase. It goes from the solidus to the allotropic transformation into the HCP\_A3  $\epsilon$  phase in Co-rich side of the diagram. By modelling separately the magnetic and non-magnetic contributions to the Gibbs energy, Guillermet [12] carried out a CALPHAD Co–Ni system assessment (**Fig 2**).

The Ni–W system was studied by various authors and discrepancies in experimental observations arose. Indeed, an intermetallic phase of composition NiW was observed by Walsh and Donachie [15] and later by Hofmann [16] with diffusion couple experiments and heat-treated alloys respectively. Poulsen *et al.* [17] claimed observing at equilibrium the intermetallic phase  $\text{NiW}_2$ , along with the NiW phase, in sintered samples made of W wires surrounded by a Ni matrix. The indexations performed by these authors from X-ray diffraction were judged as incoherent by Cury *et al.* [18] who did not detect these intermetallic phases at  $950^\circ\text{C}$  for any of the sintered, arc-melted or induction-melted alloys. Cury *et al.* found very good agreement in terms of position and relative intensity between the XRD patterns obtained by Hofmann [16], Poulsen *et al.* [17], Walsh and Donachie [15] and a simulated  $\text{Ni}_6\text{W}_6\text{C}$  pattern. Cury *et al.* concluded that NiW and  $\text{NiW}_2$  were misidentified with the  $\text{Ni}_6\text{W}_6\text{C}$  and  $\text{Ni}_2\text{W}_4\text{C}$  carbides whose formation is favored by C contamination of surfaces, a key point in case of diffusion couple experiments. Finally, it was concluded that the only stable intermetallic phase present in the Ni–W system was the body-centered tetragonal phase  $\text{Ni}_4\text{W}$  (s.g.  $I4/m$  -  $\text{MoNi}_4$  type -  $D1_a$ ). A thermodynamic assessment, performed by P. Gustafson *et al.* [4] in 1986, included the both non-existing intermetallic phases NiW and  $\text{NiW}_2$ . More recently, I. Isomäki *et al.* [5] proposed a new modeling of the Ni–W system (**Fig 3**) taking consideration of Cury *et al.* results on stable intermetallic phases. Authors also performed DFT calculations combined to phonon calculations to evaluate stability of several compounds. They confirmed the presence of three intermetallic structures on the convex-hull: the body-centered tetragonal phase  $\text{Ni}_4\text{W}$ ; the orthorhombic  $\text{Ni}_3\text{W-DO}_a$  phase (s.g.  $Pmmm$ ,  $\text{Cu}_3\text{Ti}$  prototype considered here as  $\text{DO}_a$ ); and the  $\text{Ni}_8\text{W}$  compound with martensitic-like Bravais lattice (s.g.  $I4/mmm$  -  $\text{NbNi}_8$  type). However the intermetallic phases  $\text{Ni}_3\text{W-DO}_a$  and  $\text{Ni}_8\text{W}$  were experimentally observed only

in extreme conditions [19,20] and their thermodynamic stability under normal condition remains uncertain.

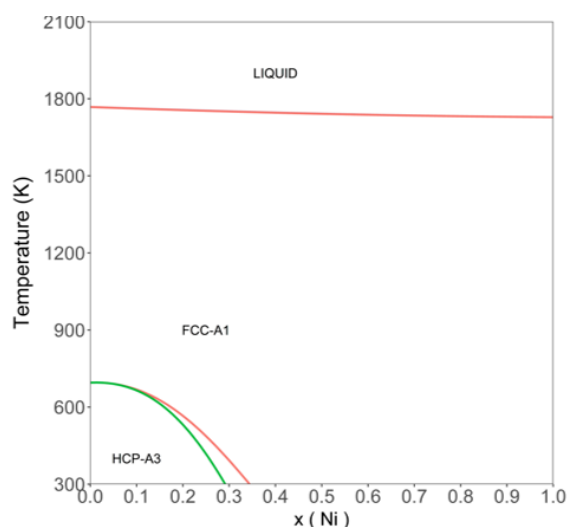


**Fig 2.** Co-Ni phase diagram from Guillermet's CALPHAD model [12]

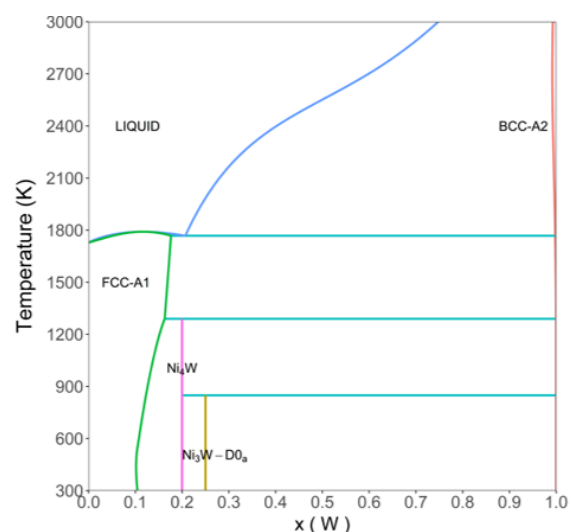


**Fig 3.** Ni-W phase diagram from Isomäki et al. CALPHAD model [5]

The Co–W binary system was evaluated extensively [6–11] with two intermetallic phases named  $\text{Co}_3\text{W}-D0_{19}$  (s.g.  $P63/mmc$  –  $\text{Ni}_3\text{Sn}$  type -  $D0_{19}$ ) and  $\text{Co}_7\text{W}_6-\mu$  (or  $\mu$  phase, s.g.  $R-3m$  –  $\text{Fe}_7\text{W}_6$  type -  $D8_5$ ) whose decomposition invariant temperatures were measured as  $1093^\circ\text{C}$  [21] and  $1689^\circ\text{C}$  [22] respectively. Sato *et al.* [8] simulated the  $\text{Co}_3\text{W}-D0_{19}$  phase with two sublattices allowing a solubility range and could well reproduce the Co-rich composition side of the intermetallic phase measured in their work. On the contrary, Guillermet [6] chose to model the  $\text{Co}_3\text{W}-D0_{19}$  phase as a stoichiometric compound. The  $\text{Co}_7\text{W}_6-\mu$  phase shows a wider homogeneity range and was modelled, for simplification purposes, with three sublattices by several authors [6–10]. J-M. Joubert and N. Dupin [23] showed the need of different occupancies on the two Wyckoff positions with coordination number 12 for the  $\text{Co}_7\text{W}_6-\mu$  phase (3a and 18h) and therefore recommended the use of a 4 sublattices model. Pure Co magnetic contribution to the Gibbs energy is significant. It must be taken into account for the description of intermetallic end-members when using formation enthalpies calculated with DFT [9–11]. The FCC\_A1 phase magnetic ordering leads to a monotectoid transformation (**Fig 4**) from paramagnetic FCC\_A1 to ferromagnetic FCC\_A1 and  $\text{Co}_3\text{W}-D0_{19}$  as predicted by Guillermet's CALPHAD assessment and confirmed experimentally by Östberg [24] and Sato *et al.* [8].

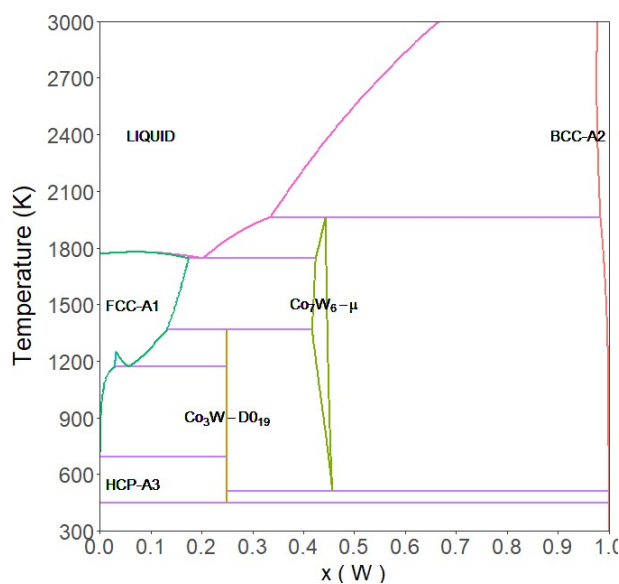


**Fig 4.** Co-W phase diagram drawn from Guillermet's CALPHAD modeling [6].

The Co-Ni-W ternary system was assessed in the late eighties by Guillermet [13] and the calculated isothermal section at 1000°C is proposed on **Fig 5**.

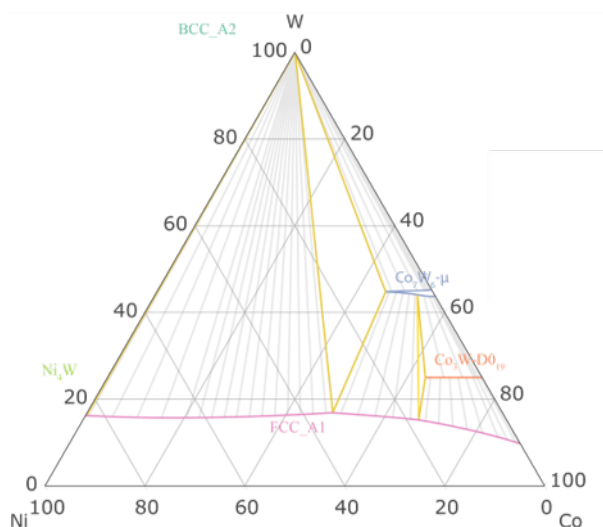


**Fig 5.** Calculated isothermal section at 1000°C according to Guillermet's assessment [13].

At that time the experimental measurements on the system were very scarce and some unpublished works carried out at the Royal Institute of Technology in Stockholm were used for parameters optimization. Sources for experimental data obtained at 1300°C and 1400°C by several authors could not be all verified. Tungsten content of the Co<sub>7</sub>W<sub>6</sub>-μ phase as modelled by Guillermet [13] appears quite low as compared to experimental measurements [25]. Discrepancies at 1000°C from Shipovskov *et al.* [26] experimental results stood out. Indeed, binary phase domains were found from the CALPHAD model located at compositions where ternary phase domains were experimentally found and inversely.

Also, the ternary domain FCC\_A1 + Co<sub>7</sub>W<sub>6</sub>-μ + Co<sub>3</sub>W-DO<sub>19</sub> defined by Guillermet was too narrow as compared to Shipovskov's experimental results.

Some years later, Zhu *et al.* [14] built diffusion multiples in the Co–Ni–W system which underwent long annealing heat treatments at 800°C and 900°C for 2200 hours and 1010 hours respectively. Diffusion multiples suffered from carbon impurity which formed Ni<sub>2</sub>W<sub>4</sub>C and Ni<sub>6</sub>W<sub>6</sub>C carbides at the interface with tungsten and prevented the measurement of most tie-lines. However, tie-lines obtained after EPMA measurements exhibited nickel solubility in Co<sub>3</sub>W-DO<sub>19</sub> ranging from 13 at% at 900°C to 62 at% at 800°C. These values strongly differed from the ones issued from Guillermet's modeling that were respectively 6.5 at% and 29 at% [13].

Consequently, the available thermodynamic description of the ternary Co–Ni–W system is inconsistent mostly at temperatures lower than 1300°C where experimental measurements are both scarce and in disagreement. From the results presently obtained and the past investigations, the phases considered for the Co–Ni–W ternary system are listed in

**Table 1.**

Phase name	Space Group	Prototype	Number of sublattices
FCC_A1 (γ)	<i>Fm-3m</i>	Cu	1
BCC_A2 (α)	<i>Im-3m</i>	W	1
HCP_A3 (ε)	<i>P6<sub>3</sub>/mmc</i>	Mg	1
Ni <sub>4</sub> W	<i>I4/m</i>	Ni <sub>4</sub> Mo	2
(Co,Ni) <sub>3</sub> W-DO <sub>19</sub>	<i>P6<sub>3</sub>/mmc</i>	Ni <sub>3</sub> Sn	2
(Co,Ni) <sub>3</sub> W-DO <sub>a</sub>	<i>Pmmn</i>	Cu <sub>3</sub> Ti	3
Co <sub>7</sub> W <sub>6</sub> -μ	<i>R-3m</i>	Fe <sub>7</sub> W <sub>6</sub>	5

**Table 1.** Phases reported in the Co–Ni–W ternary system.

### 3. Experimental procedure

Samples were prepared from pure Co, Ni and W powders which chemical compositions are described in **Table 2**. The compositions of most samples (except sample 51W) were chosen with a fixed W (30 at%) and variable Ni content (from 15 to 40 at%, see **Table 3**). The powders were blended for 30 min to get homogeneous distribution of the elements and then milled with Co–Ni–W WHA balls for 30 min. Milled powders were isostatically pressed at 190 MPa. Samples were solid-state sintered at 1440°C for one hour under a pure hydrogen atmosphere to reduce the oxide layer on the powder surface. The samples were then cooled at a controlled 5°C.min<sup>-1</sup> rate down to 800°C and then, inertially.

Element	Maximum impurity content (ppm)		
	Ni	Co	W
C	800	300	30
S	10	50	5
Fe	100	200	100
Ni	/	100	/
Ca	/	100	/
Na	/	100	10
Si	/	100	30
Mo	/	/	30

**Table 2.** Chemical composition of elemental powders used in this work.

Sample identification	Initial Composition (at%)			Phases identified by XRD	Composition determined by EPMA (at%)		
	Co	Ni	W		Co <sub>(σ)</sub>	Ni <sub>(σ)</sub>	W <sub>(σ)</sub>
Ni15	55	15	30	Co <sub>7</sub> W <sub>6</sub> -μ	46.86 <sub>(0.19)</sub>	8.51 <sub>(0.32)</sub>	44.63 <sub>(0.26)</sub>
				Co <sub>3</sub> W-D0 <sub>19</sub>	58.05 <sub>(0.58)</sub>	18.94 <sub>(0.65)</sub>	23.00 <sub>(0.32)</sub>
Ni17.5	53.5	17.5	30	Co <sub>7</sub> W <sub>6</sub> -μ	/	/	/
				Co <sub>3</sub> W-D0 <sub>19</sub>	/	/	/
Ni20	50	20	30	Co <sub>7</sub> W <sub>6</sub> -μ	43.11 <sub>(0.53)</sub>	11.43 <sub>(0.46)</sub>	45.46 <sub>(0.17)</sub>
				Co <sub>3</sub> W-D0 <sub>19</sub>	52.53 <sub>(0.43)</sub>	23.91 <sub>(0.34)</sub>	23.56 <sub>(0.13)</sub>
Ni21.5	48.5	21.5	30	Co <sub>7</sub> W <sub>6</sub> -μ	43.37 <sub>(0.69)</sub>	11.28 <sub>(0.71)</sub>	45.35 <sub>(0.24)</sub>
				Co <sub>3</sub> W-D0 <sub>a</sub>	50.66 <sub>(0.45)</sub>	25.75 <sub>(0.44)</sub>	23.59 <sub>(0.10)</sub>
Ni23	47	23	30	Co <sub>7</sub> W <sub>6</sub> -μ	/	/	/
				Co <sub>3</sub> W-D0 <sub>a</sub>	/	/	/
Ni25	45	25	30	Co <sub>7</sub> W <sub>6</sub> -μ	40.13 <sub>(0.36)</sub>	14.32 <sub>(0.21)</sub>	45.55 <sub>(0.21)</sub>
				Co <sub>3</sub> W-D0 <sub>a</sub>	47.08 <sub>(0.27)</sub>	29.60 <sub>(0.27)</sub>	23.32 <sub>(0.07)</sub>
Ni30	40	30	30	Co <sub>7</sub> W <sub>6</sub> -μ	35.51 <sub>(0.61)</sub>	17.78 <sub>(0.62)</sub>	46.71 <sub>(0.42)</sub>
				Co <sub>3</sub> W-D0 <sub>a</sub>	40.58 <sub>(0.27)</sub>	35.10 <sub>(0.32)</sub>	24.32 <sub>(0.31)</sub>
Ni40	30	40	30	Co <sub>7</sub> W <sub>6</sub> -μ	32.32 <sub>(0.59)</sub>	21.23 <sub>(0.40)</sub>	46.46 <sub>(0.32)</sub>
				Co <sub>3</sub> W-D0 <sub>a</sub>	31.70 <sub>(0.38)</sub>	44.46 <sub>(0.34)</sub>	23.84 <sub>(0.09)</sub>
				BCC_A2	-*	-*	-*
51W	23.1	52.1	24.8	FCC_A1	24.39 <sub>(0.54)</sub>	59.00 <sub>(1.23)</sub>	16.61 <sub>(0.41)</sub>
				Co <sub>3</sub> W-D0 <sub>a</sub>	24.09 <sub>(1.27)</sub>	52.49 <sub>(0.98)</sub>	23.42 <sub>(0.41)</sub>
				BCC_A2	-*	-*	-*

\* : High uncertainties on EPMA measurements.

/ : EPMA measurements not performed on the sample.

**Table 3.** Samples initial composition and composition of the phases formed in Co–Ni–W powder mixtures after 720h at 1000°C.

A 15 mm diameter slice of each as-sintered cylinder was cut using electrical discharge machining. Slices were wrapped in tantalum foils. Samples were then sealed in a silica bulb under residual argon

atmosphere and underwent a 1500 hours long annealing heat treatment at  $800\pm 5^\circ\text{C}$  or a 720 hours long annealing heat-treatment at  $1000^\circ\text{C}\pm 5^\circ\text{C}$  followed by rapid quenching in water.

Afterwards each slice was cut in two pieces to conduct different characterizations. Half of the samples was resin-mounted, grinded and meticulously polished (finish with colloidal silica solution) to enable EDS and WDS composition measurements. Scanning Electron Microscopy (SEM) on a Zeiss Merlin Compact was conducted under 15 kV accelerating voltage to observe the samples microstructure. EDS point measurements were performed with an Oxford Instruments X-Max<sup>N</sup> detector using electronic standards to approximate the composition of the phases involved in the equilibria at  $800^\circ\text{C}$  and  $1000^\circ\text{C}$ . In order to measure the chemical compositions accurately, the samples heat treated at  $1000^\circ\text{C}$  were also characterized using electron probe microanalysis (EPMA) and pure standards for the 3 elements (Co, Ni and W). The measurements were carried out on a SX100 Cameca microprobe with a 18 kV accelerating voltage, a 60 nA probe current, LiF monochromators for Co and Ni  $K_\alpha$  radiations and a TAP monochromator for W  $M_\alpha$  radiation. Quantitative procedure for analysing the samples used the PAP  $\Phi(\rho z)$  model from Pouchou and Pichoir [27].

Sample N, of specific composition (Ni/Co ratio of 0.7 and 25.5 at% W) was also included in the heat treatments at  $1000^\circ\text{C}$ . From this sample, a thin foil was prepared using Focused Ion Beam and a JEOL 2010 LaB6 Transmission Electron Microscope operated at 200kV was used in order to characterize the  $\text{Co}_3\text{W-D0}_a$  like intermetallic phase using Electron Diffraction.

The other half of samples treated at  $1000^\circ\text{C}$  were crushed into powders at room temperature using a dedicated jar along with a ball both made of tungsten carbide. The powders were sieved to reach a particle size below 20  $\mu\text{m}$  in diameter. Sieved powder was suspended in 5 mL ethanol with silicon powder (XRD internal reference) and the resulting suspension was sonicated for 5 minutes. Droplets of this suspension were deposited on a zero background monocrystalline corundum substrate for XRD. The diffractograms were acquired on a Bruker D8 advance using the Cu radiation ( $\lambda_{\alpha 1} = 1,54060 \text{ \AA}$  and  $\lambda_{\alpha 2} = 1,54439 \text{ \AA}$ ) for 8 hours with a  $2\theta$  step of  $0.008^\circ$  in  $\theta$ - $\theta$  Bragg Brentano geometry over the  $2\theta$  range  $10$ - $60^\circ$ . The divergence slits were fixed to  $0.3^\circ$  opening for radial divergence and a 4mm mask was used for axial divergence. Le Bail refinement was performed with the Fullprof software [28] to confirm phase identification and to measure the lattice parameters of the intermetallic phases. Le Bail refinements were conducted in isotropic conditions to achieve a satisfactory profile matching. The samples heat treated at  $800^\circ\text{C}$  were characterized as bulk specimen after removing surface layers and polishing to sharply reduce the surface roughness. The diffractograms were acquired in the same conditions as the ones selected for samples heat treated at  $1000^\circ\text{C}$ .

Sample identification	Initial Composition (at%)			Phases identified by XRD	Composition determined by EDS (at%)		
	Co	Ni	W		Co <sub>(σ)</sub>	Ni <sub>(σ)</sub>	W <sub>(σ)</sub>
Ni20	50	20	30	Co <sub>7</sub> W <sub>6</sub> - μ	43.11 <sub>(0.28)</sub>	11.50 <sub>(0.28)</sub>	45.39 <sub>(0.19)</sub>
				Co <sub>3</sub> W-DO <sub>19</sub>	52.86 <sub>(1.10)</sub>	22.62 <sub>(1.26)</sub>	24.52 <sub>(0.33)</sub>
Ni21.5	48.5	21.5	30	Co <sub>7</sub> W <sub>6</sub> - μ	/	/	/
				Co <sub>3</sub> W-DO <sub>19</sub>	/	/	/
Ni23	47	23	30	Co <sub>7</sub> W <sub>6</sub> - μ	41.22 <sub>(0.59)</sub>	12.94 <sub>(0.70)</sub>	45.84 <sub>(0.22)</sub>
				Co <sub>3</sub> W-DO <sub>19</sub>	49.57 <sub>(0.54)</sub>	25.78 <sub>(0.70)</sub>	24.65 <sub>(0.32)</sub>
Ni25	45	25	30	Co <sub>7</sub> W <sub>6</sub> - μ	39.91 <sub>(0.49)</sub>	14.23 <sub>(0.49)</sub>	45.86 <sub>(0.28)</sub>
				Co <sub>3</sub> W-DO <sub>19</sub>	47.05 <sub>(0.61)</sub>	28.70 <sub>(0.76)</sub>	24.24 <sub>(0.64)</sub>
Ni30	40	30	30	Co <sub>7</sub> W <sub>6</sub> - μ	35.59 <sub>(0.48)</sub>	17.99 <sub>(0.47)</sub>	46.42 <sub>(0.41)</sub>
				Co <sub>3</sub> W-DO <sub>a</sub>	41.07 <sub>(0.53)</sub>	34.43 <sub>(0.73)</sub>	24.50 <sub>(0.50)</sub>
Ni40	30	40	30	BCC_A2	-*	-*	-*
				Co <sub>3</sub> W-DO <sub>a</sub>	32.29 <sub>(0.34)</sub>	43.14 <sub>(0.53)</sub>	24.57 <sub>(0.61)</sub>
Ni54.5	15.5	54.5	30	BCC_A2	-*	-*	-*
				Co <sub>3</sub> W-DO <sub>a</sub>	16.84 <sub>(0.47)</sub>	58.68 <sub>(0.34)</sub>	24.48 <sub>(0.42)</sub>

\* : Uncertainties on EDS measurements are high because of the size of the phases and operating conditions leading to a risk of an interaction volume bigger than the size of the phase.

/ : EDS measurements not performed on the sample.

**Table 4.** Samples initial composition and composition of the phases formed in Co–Ni–W powder mixtures after 1500h at 800°C.

TGA-DSC analyses were performed on the crushed powders of samples heat treated at 1000°C. For all analyses, the TGA/DSC3+ device from Mettler-Toledo was used and samples were put into 150 μL alumina crucibles. Temperature calibration was achieved with the melting temperature measurements of In, Al and Au standards. Analyses were run under a purified argon flow using a type N Subtronic purifier and the tested sample masses were very close to each other. The cycle consisted in a 20°C.min<sup>-1</sup> heating ramp to 950°C, an isothermal dwell at 950°C for 30 minutes followed by a 5°C.min<sup>-1</sup> heating ramp to reach 1200°C. The decomposition onset temperature of the Co<sub>3</sub>W like phases was assessed as the temperature for which a fixed value for the baseline deviation was reached as illustrated in **Fig 9.a**. TGA-DSC analyses were also done for several samples heat treated at 800°C on bulk specimens. The isothermal dwell was set at 780°C for 30 minutes and was followed by a 5°C.min<sup>-1</sup> heating ramp up to 1200°C.

First principle calculations were performed using the Density Functional Theory (DFT) under the General Gradient Approximation (GGA) with the Perdew-Burke-Ernzerhof (PBE) exchange-correlation energy functionals expression [29]. The VASP code was used with the Projector Augmented Wave (PAW) approach [30]. The energy cut-off for the PAWs was set to 600 eV. The ZenGen script [31] was used to automatically organize the input files for every end-member and adopt progressive relaxation steps. Magnetic moments were calculated using a spin polarized model once all relaxation steps for the non-magnetic state were achieved. The irreducible Brillouin zone (BZ) was sampled using high-density k meshing of 0.05 Å<sup>-1</sup> points for each primitive cell. The formation enthalpy at 0 K of every ternary

end-members for the  $\text{Co}_7\text{W}_6\text{-}\mu$  phase with its 5 sublattices ( $3^5=243$  configurations), the  $\text{Co}_3\text{W-}D0_a$  phase with its 3 sublattices ( $3^3=27$  reduced to 14 unique configurations, since the crystal sites present similar environment and the permutation of atoms leads to some degenerated configurations) and the  $\text{Co}_3\text{W-}D0_{19}$  phase with its 2 sublattices ( $3^2=9$  configurations) were calculated by total energy differences of compound with their weighted elements in their stable reference state. Special Quasirandom Structure (SQS) using MCSQS [32,33] tool were considered to generate cells with a mixing of atoms for the  $\text{Co}_3\text{W-}D0_a$  phase to compare relative stability of partial occupancies. The clusters considered for the SQS study were limited to 9 pairs, 7 triangles and 4 tetrahedra to design 48 to 72-atoms SQS cells depending of the studied compositions.

## 4. Results and discussions

### 4.1. Phase Equilibria

X-rays diffraction was performed on each sample. The diffractograms obtained from suspended powders deposition for sample Ni15 to sample Ni25 are shown in **Fig 6**. Profile matchings achieved in isotropic conditions with Fullprof were characterized by the reliability R-factors related to points with Bragg contributions corrected for background. These R-factors are characterized by  $R_p < 25$ ,  $R_{wp} < 18$  and  $\text{Chi}2 < 4$ .

For low Ni content (samples Ni15, Ni17.5 and Ni20), the  $\text{Co}_7\text{W}_6\text{-}\mu$  phase was identified together with  $\text{Co}_3\text{W-}D0_{19}$  at  $1000^\circ\text{C}$ . According to diffraction peaks positions and Le Bail refinement, the later phase crystallizes in the  $P6_3/mmc$  space group with  $a=5.125 \text{ \AA}$ ,  $c=4.148 \text{ \AA}$  as refined lattice parameters for sample Ni20.

A change is observed in diffraction peaks existence and position between sample Ni20 and sample Ni21.5. This is visible from the triplet found between  $25^\circ$  and  $30^\circ 2\theta$  or the doublet around  $35^\circ 2\theta$  on **Fig 6**. These diffraction peaks can be attributed by Le Bail refinement to a  $\text{Co}_3\text{W-}D0_a$  phase. This phase is isostructural to the  $\text{Ni}_3\text{Mo}$  compound and it crystallizes in the  $Pm\bar{m}n$  space group with  $a=5.113 \text{ \AA}$ ,  $b=4.141 \text{ \AA}$  and  $c=4.463 \text{ \AA}$  as refined lattice parameter for sample Ni21.5. Consequently, X-ray diffraction analysis reveals a structural transition at  $1000^\circ\text{C}$  from  $\text{Co}_3\text{W-}D0_{19}$  to  $\text{Co}_3\text{W-}D0_a$  caused by nickel addition with nominal concentration from 20 at% to 21,5 at%.

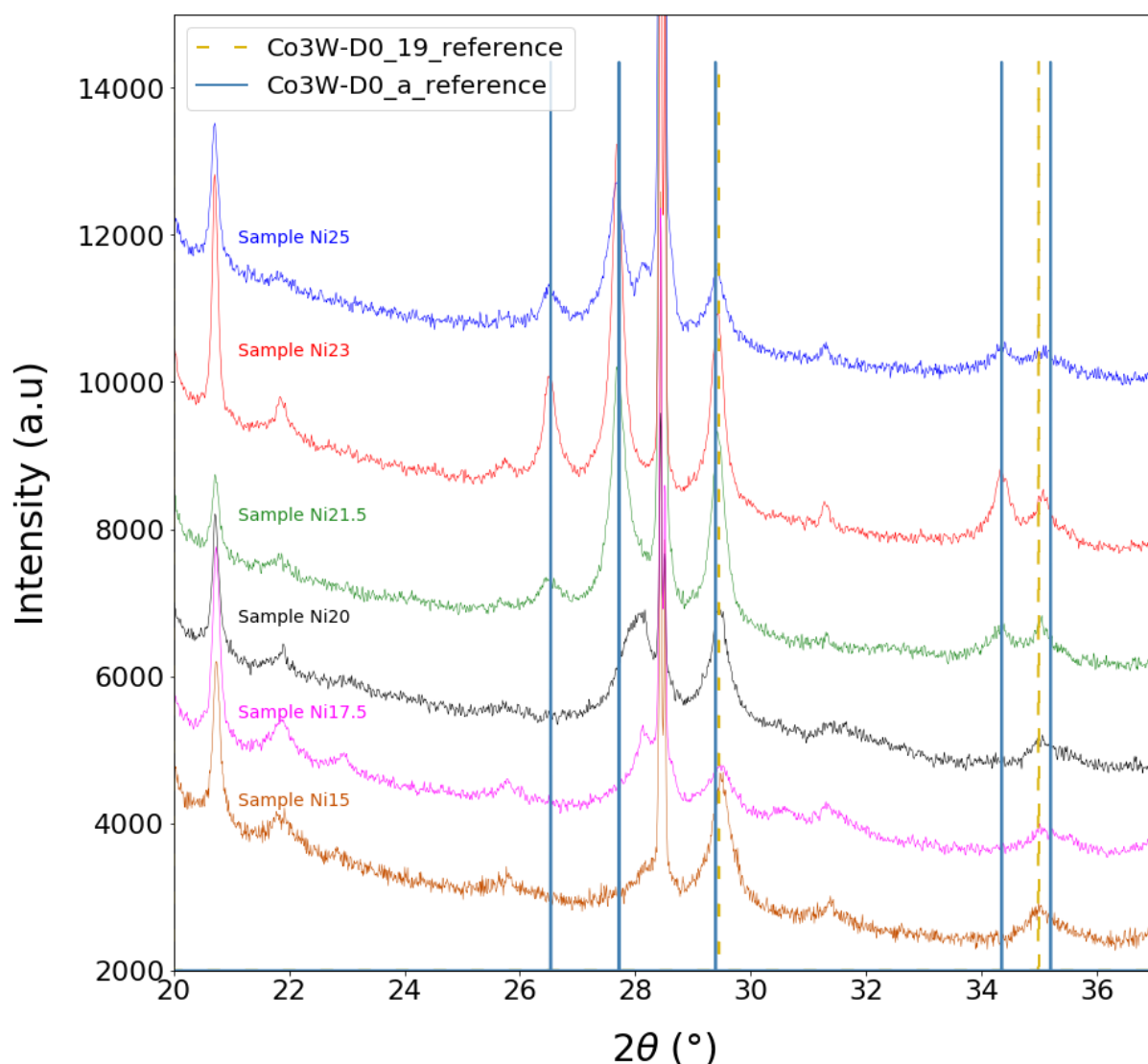


**Fig 6.** Evolution of powder diffractograms obtained in a series of W–Ni–Co samples with constant 30 at% W and increasing Ni content after 720 h at 1000 °C. Samples are crushed after heat treatment and sieved powders deposited on monocryalline corundum substrate. Characteristic lines for  $\text{Co}_3\text{W-D0}_a$  and  $\text{Co}_3\text{W-D0}_{19}$  structures are added for lecture. Diffraction peak at  $20.7^\circ 2\theta$  is from  $\text{Co}_7\text{W}_6\text{-}\mu$  phase. Addition of Si XRD internal reference is observed at  $28.47^\circ 2\theta$ .

Sample N (heat treated at  $1000^\circ\text{C}$ ) TEM measurements confirmed the  $\text{Co}_3\text{W-D0}_a$  structure. The FIB sample location is illustrated on **Fig 7.(a)** and was extracted in an area containing only  $\text{Co}_3\text{W-D0}_a$  phase. As  $\text{Co}_3\text{W-D0}_a$  and  $\text{Co}_3\text{W-D0}_{19}$  present very similar structures, most of the electron diffraction pattern recorded could be indexed with both phases, except the  $\langle 1\bar{1}0 \rangle$  presented in **Fig 7.(c)**. This specific orientation allowed to discriminate between the two phases, since the (110) and (00 $\bar{1}$ ) planes of the  $\text{Co}_3\text{W-D0}_a$  structure are in diffraction conditions. Triplet of plans {101} are used in X-ray diffraction analysis to distinguish between the two phases as the diffractograms were very similar and many peaks were convolved with the ones from the  $\text{Co}_7\text{W}_6\text{-}\mu$  phase.

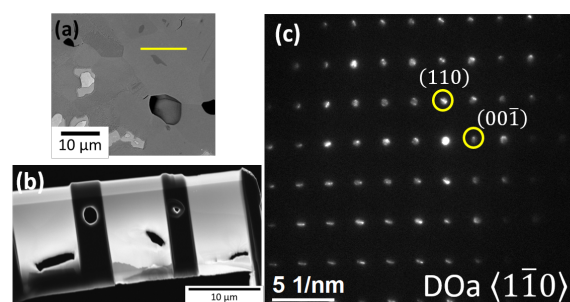


**Fig 7.** (a) Location of the extraction zone of the FIB sample used for electron diffraction study, (b) SEM-SE observation of the thin foil and (c) Small Area Electron Diffraction pattern of one of the grain oriented  $\langle 1\bar{1}0 \rangle$  and indexed as  $\text{Co}_3\text{W-D0}_a$  phase.

The annealing heat treatments at 800°C and 1000°C led to thermodynamic equilibrium as it is illustrated in **Fig 8** for sample Ni40. Three phases in contact with each other are observed at 1000°C, illustrating the existence of a three-phase equilibrium. X-rays powder diffraction performed on the crushed sample allows the identification of the phases BCC\_A2,  $\text{Co}_3\text{W-D0}_a$  and  $\text{Co}_7\text{W}_6\text{-}\mu$ . EPMA measurements reveal that the maximum Ni solubility in the  $\text{Co}_7\text{W}_6\text{-}\mu$  phase is 21.23 at%.Ni at 1000°C (**Table 3**). In addition, this sample emphasizes the stability of a  $\text{Co}_3\text{W-D0}_a$  structure with a Ni content of 44.46 at%.

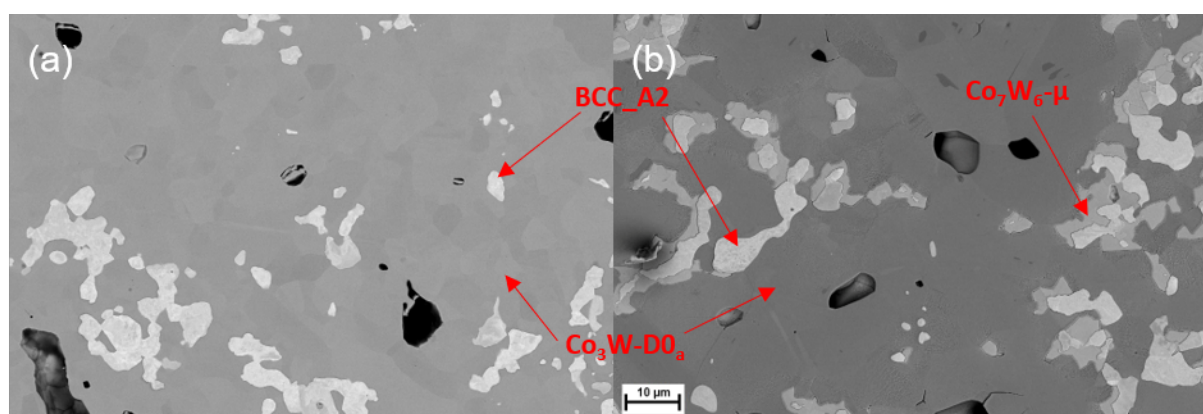


**Fig 8.** Microstructure of sample Ni40 after 1500 h at 800 °C (a) and after 720 h at 1000°C (b) observed with SEM in BSE mode (magnification x1000).

Experimental measurements in **Table 3** confirm the stability of the BCC\_A2+ $\text{Co}_3\text{W-D0}_a$  binary phase domain at 1000°C as well as the two ternary phase domains BCC\_A2+ $\text{Co}_3\text{W-D0}_a$ +FCC\_A1 and BCC\_A2+ $\text{Co}_3\text{W-D0}_a$ + $\text{Co}_7\text{W}_6\text{-}\mu$ . From EPMA compositions for both  $\text{Co}_3\text{W-D0}_a$  and  $\text{Co}_3\text{W-D0}_{19}$ , a shift from stoichiometry is observed since the tungsten content is slightly lower than 25 at%. (**Table 3**). There is also a trend for an increase in tungsten content of the  $\text{Co}_7\text{W}_6\text{-}\mu$  phase in equilibrium with  $\text{Co}_3\text{W-D0}_a$  or  $\text{Co}_3\text{W-D0}_{19}$  with nickel addition. The composition obtained at 1000°C with EDS were in very good agreement with the ones measured with EPMA. Thus, EPMA measurements for samples heat treated at 800°C were not necessary provided that EDS measurements were performed in the same conditions as the ones already compared with EPMA at 1000°C.

Composition measurements and phase identification obtained for the samples treated at 800°C (**Table 4**) show a decrease in the maximum Ni dissolution for the  $\text{Co}_7\text{W}_6\text{-}\mu$  phase (<21,23 at% Ni) and a shift

towards lower Co content for the ternary phase domain BCC\_A2+Co<sub>3</sub>W-D0<sub>a</sub>+FCC\_A1 if compared with samples treated at 1000°C.

TGA-DSC analyses on samples heat treated at 1000°C defined the decomposition onset temperature of the Co<sub>3</sub>W-like phases as the kinetics for the monovariant reactions are fast. The decomposition onset temperature for sample Ni30 heat treated at 1000°C is shown on **Fig 9.a** by a vertical line. The evolution in the onset temperatures as a function of the samples nominal Ni/Co ratio is shown on **Fig 9.b**. In this figure, a previous measurement is included and was obtained on a sample richer in Co than sample Ni20, obtained from an arc melted pellet heat treated at 1000°C. The phase transition between Co<sub>3</sub>W-D0<sub>19</sub> and Co<sub>3</sub>W-D0<sub>a</sub> is conspicuous since the onset decomposition temperature first decreases with low Ni addition and then increases when the nominal Ni content is higher than 21.5 at%. Indeed, there is a fall in the Co<sub>3</sub>W-D0<sub>19</sub> decomposition onset temperature from 1093°C in the Co–W binary system to 1035°C for sample Ni20 heat treated at 1000°C. The decomposition onset temperature for the Co<sub>3</sub>W-D0<sub>a</sub> phase from sample Ni25 to sample Ni40 around 1045°C is stable. The onset decomposition temperature for higher Ni content decreases as illustrated for sample 51W.

Samples Ni21.5, Ni23 and Ni25 heat treated at 800°C were studied with TGA-DSC to show the Co<sub>3</sub>W-D0<sub>19</sub> to Co<sub>3</sub>W-D0<sub>a</sub> phase transition between 800°C and 1000°C. As illustrated in **Fig 10** for sample Ni25, the DSC curves did not allow the identification of any phase transition below 1000°C. It may be caused either by sluggish kinetics below 1000°C or by the nature of the phase transition. The later may be of the second order and thus corresponds to an athermal structure transition. Sluggish kinetics were confirmed for the Co<sub>3</sub>W-D0<sub>a</sub> decomposition with sample Ni54.5 (Ni/Co=3.52) treated at 800°C. The onset decomposition temperature was measured around 995°C, which is inconsistent with EPMA measurements of sample 51W (Ni/Co=1.83) heat treated at 1000°C. Phase change kinetic limitations was also observed with sample Ni40 heat treated at 800°C for which two thermal phenomena were expected from structural data shown in **Table 3** and **Table 4**. However, there was only the Co<sub>3</sub>W-D0<sub>a</sub> phase decomposition that was detected with the DSC curve. The onset decomposition temperatures of samples heat treated at 1000°C must be considered as maximum temperatures for phase transition in thermodynamic assessment. Therefore, delay in temperature due to sluggish kinetics must be accounted for.

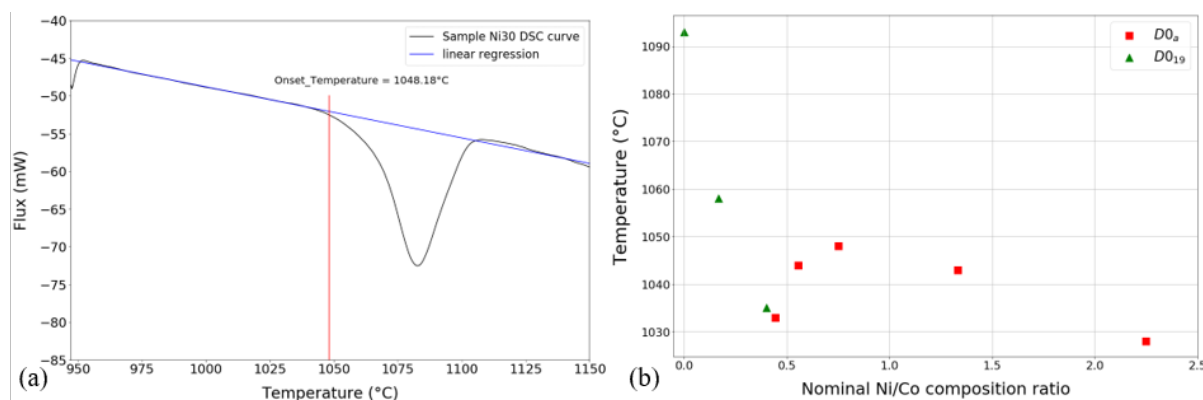


**Fig 9.** (a) DSC onset decomposition temperature assessment for sample Ni30 heat treated 720 hours at 1000°C and (b) onset decomposition temperature evolution of  $\text{Co}_3\text{W}$  like phases as a function of the nominal Ni/Co composition ratio obtained from samples equilibrated at 1000°C.

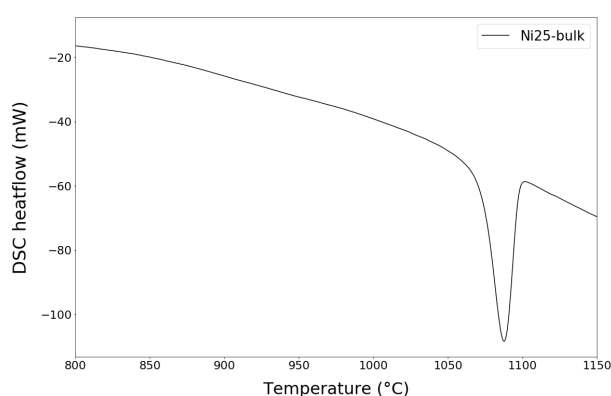


**Fig 10.** DSC curve of sample Ni25 heat treated at 800°C.

An isothermal section at 1000°C of the ternary Co–Ni–W system is suggested in **Fig 11**. The change in tie-line orientation between sample Ni20 and sample Ni21.5 (as well as a common measured composition for the  $\text{Co}_7\text{W}_6\text{-}\mu$  phase for both samples) draw a thin  $\text{Co}_7\text{W}_6\text{-}\mu + \text{Co}_3\text{W-D0}_a + \text{Co}_3\text{W-D0}_{19}$  ternary phase domain perimeter. It is consistent with TGA-DSC and XRD measurements performed on samples heat-treated at 1000°C. The sample compositions Ni17.5, Ni20, Ni21.5, Ni23 were used to verify experimentally the  $\text{Co}_7\text{W}_6\text{-}\mu + \text{Co}_3\text{W-D0}_a + \text{Co}_3\text{W-D0}_{19}$  ternary phase domain existence. Ternary phase domain occurrence is supported in this work, even though the attempt to check its existence was unfruitful. XRD and EDS measurements performed on samples heat-treated at 800°C and 1000°C as well as TGA-DSC analyses show a shift towards the Co rich side of the Co–Ni–W system of the expected ternary phase domain ( $\text{Co}_7\text{W}_6\text{-}\mu + \text{Co}_3\text{W-D0}_a + \text{Co}_3\text{W-D0}_{19}$ ) when the temperature increases. From these observations, an invariant phase transformation  $\text{Co}_3\text{W-D0}_a + \text{Co}_3\text{W-D0}_{19} \leftrightarrow \text{FCC\_A1} + \text{Co}_7\text{W}_6\text{-}\mu$  seems to occur close to 1030°C and below 21.5 at% Ni. More likely the ternary phase domain  $\text{FCC\_A1} + \text{Co}_7\text{W}_6\text{-}\mu + \text{Co}_3\text{W-D0}_a$  should shift quickly towards Ni rich side of the Co–Ni–W system when temperature increases beyond 1030°C.

We can affirm that the highest Ni/Co nominal ratio to avoid precipitation of any intermetallic phase between 800°C and 1000°C is higher than 3.52 in the Co–Ni–W system. This is in agreement with the results from Zhu et al. [14] but is in contradiction with the CALPHAD modeling from Guillermet [13].

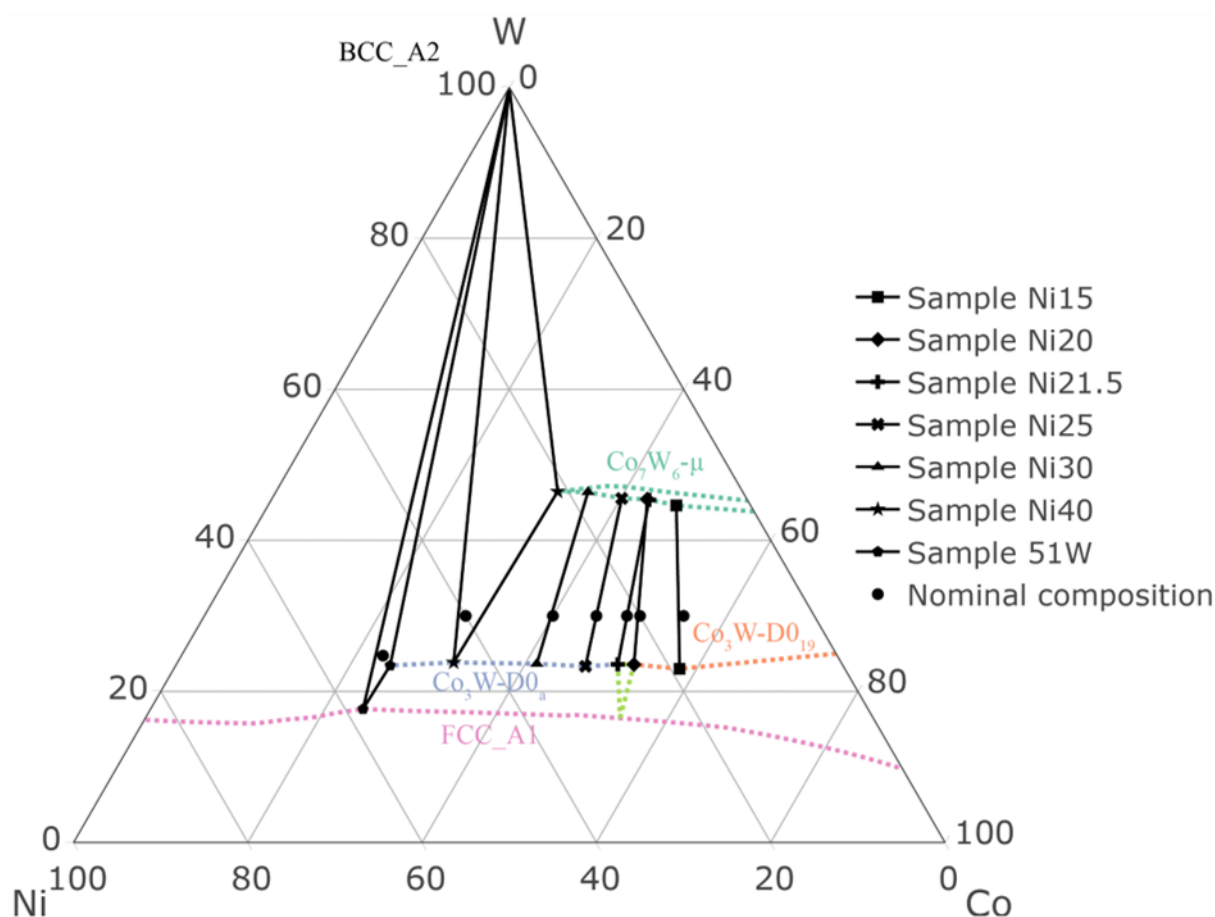


**Fig 11.** Experimental EMPA composition measurements of samples heat treated 720 hours at 1000°C superimposed on the proposed isothermal section of the W–Ni–Co system at 1000°C.

#### 4.2. DFT calculations and phase stability

Phase	Composition			Lattice parameters (Å)			Atomic positions			
	x(Co)	x(Ni)	x(W)	a	b	c	Site label	x	y	z
<b>Co<sub>3</sub>W-D0<sub>19</sub></b>	0.75	0	0.25	5.0965	5.0965	4.0835	6h-Co	0.162	0.324	0.75
							2c-W	1/3	2/3	0.25
<b>Co<sub>3</sub>W-D0<sub>a</sub></b>	0.50	0.25	0.25	5.1653	4.0889	4.3998	4e-Co	0.25	0.00	0.672
							2a-Ni	0.25	0.25	0.182

**Table 5** summarizes the crystallographic data obtained from DFT calculation in a given ordered configuration for both Co<sub>3</sub>W-D0<sub>19</sub> and Co<sub>3</sub>W-D0<sub>a</sub>. In Co<sub>3</sub>W-D0<sub>19</sub> structure, Co and W atoms are located on Wyckoff position 6h and 2c respectively since Co<sub>3</sub>W-D0<sub>19</sub> is a thermodynamically stable ordered structure from the HCP\_A3 solid solution at 1000°C. Ni substitution to Co is expected on atomic site 6h until the solubility limit of Ni in this phase is reached. In Co<sub>3</sub>W-D0<sub>a</sub> structure, Ni and Co atoms occupy Wyckoff positions 2a and 4e respectively whereas W atoms are located on 2b Wyckoff position.

Phase	Composition			Lattice parameters (Å)			Atomic positions			
	x(Co)	x(Ni)	x(W)	a	b	c	Site label	x	y	z
<b>Co<sub>3</sub>W-D0<sub>19</sub></b>	0.75	0	0.25	5.0965	5.0965	4.0835	6h-Co	0.162	0.324	0.75
							2c-W	1/3	2/3	0.25
<b>Co<sub>3</sub>W-D0<sub>a</sub></b>	0.50	0.25	0.25	5.1653	4.0889	4.3998	4e-Co	0.25	0.00	0.672
							2a-Ni	0.25	0.25	0.182

**Table 5.** Structure comparison from DFT calculations.

Formation enthalpies for both intermetallic phases Co<sub>3</sub>W-D0<sub>a</sub> and Co<sub>3</sub>W-D0<sub>19</sub> are provided in **Table 6** and **Table 7** **Erreur ! Source du renvoi introuvable.** respectively. Formation enthalpies in Co<sub>3</sub>W-D0<sub>a</sub> of the X:A:B and X:B:A configurations were found identical when A and B atoms were swapped between sites 2a and 2b since coordination distances of the 12 nearest neighbors for sites 4e, 2a and 2b were the same. Likewise, A:B:B and B:A:A configurations led to the same formation enthalpies. This degeneracy caused the reduction from 27 to 14 unique configurations as indicated in **Table 6**.

Comparable samples	Atom on site 4e	Atom on site 2a	Atom on site 2b	x(Co)	x(Ni)	x(W)	$\Delta H$ (kJ/mol)
/	Co	Co	Co	1	0	0	-0.025
/	Co	Co	W	0.75	0	0.25	-5.215
/	Co	W	W	0.5	0	0.5	5.113
/	W	Co	W	0.25	0	0.75	32.303
/	W	Ni	W	0	0.25	0.75	25.864
/	W	Ni	Ni	0	0.5	0.5	3.479
/	Ni	Ni	W	0	0.75	0.25	-10.380
/	Ni	Ni	Ni	0	1	0	2.192
Ni23	Co	Ni	W	0.5	0.25	0.25	-6.587
51W	Ni	Co	W	0.25	0.5	0.25	-8.283
/	W	W	W	0	0	1	48.995
/	Co	Co	Ni	0.75	0.25	0	-1.869
/	Ni	Co	Co	0.5	0.5	0	-0.782
/	Ni	Ni	Co	0.25	0.75	0	0.596

**Table 6.** DFT calculated formation enthalpies for end-members of the Co<sub>3</sub>W-D0<sub>a</sub> phase.

Atom on site 6h	Atom on site 2d	x(Co)	x(Ni)	x(W)	$\Delta H$ (kJ/mol)
Co	Co	1	0	0	-0.014
Ni	Ni	0	1	0	2.345
W	W	0	0	1	48.957
Co	Ni	0.75	0.25	0	-2.260

Ni	Co	0.25	0.75	0	1.445
Co	W	0.75	0	0.25	-8.098
W	Co	0.25	0	0.75	33.145
W	Ni	0	0.25	0.75	24.102
Ni	W	0	0.75	0.25	-3.511

**Table 7.** DFT calculated formation enthalpies for end-members of the  $\text{Co}_3\text{W-DO}_{19}$  phase.

Calculated formation enthalpies at 0 K for ordered configurations are represented in **Fig 12** as a function of Ni/Co ratio for the  $\text{DO}_a$  and  $\text{DO}_{19}$  intermetallic phases along the isopleth ideal composition line between  $\text{Ni}_3\text{W}$  and  $\text{Co}_3\text{W}$ . DFT calculations demonstrate that Ni substitution for Co leads to a stability inversion favorable to  $\text{DO}_a$  formation. Consequently DFT calculations support the experimental evidence that Ni addition tends to stabilize the  $\text{DO}_a$  intermetallic phase at the expense of the  $\text{DO}_{19}$  phase in the Co–Ni–W ternary system.

For a better understanding of the Co/Ni substitution mechanism in the  $\text{Co}_3\text{W-DO}_a$  intermetallic phase, SQS calculations enabled partial sublattice site occupancy of sites 2a and 4e to be studied. Formation enthalpies calculated with SQS (

**Table 8**) for  $x(\text{Ni})=0.25$  and  $x(\text{Ni})=0.50$  show that full substitutional models with a common Ni site occupancy for sites 2a and 4e are energetically alike when compared to ordered configurations. It is also shown for  $x(\text{Ni})=0.50$  that Ni in 2a and half 4e is preferred to the ordered phase with Ni in 4e. Hence it may be assumed that substitution of Co by Ni in the  $\text{Co}_3\text{W-DO}_a$  phase proceeds by filling site 2a and when full occupancy is reached, substitution would continue on site 4e.

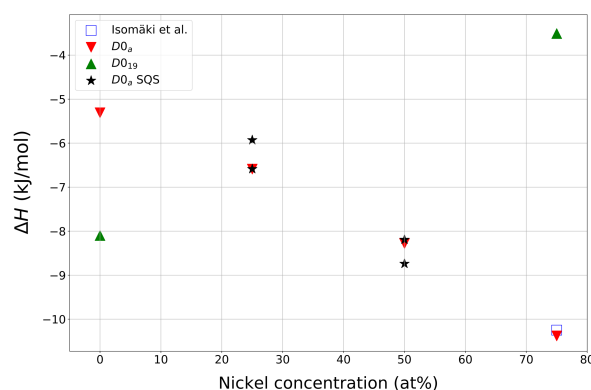


**Fig 12.** Formation enthalpy evolution calculated with DFT as a function of Ni concentration for  $\text{Co}_3\text{W-DO}_a$  and  $\text{Co}_3\text{W-DO}_{19}$  structure with a fixed 25 at% W at 0 K.

$\text{Co}_3\text{W-DO}_a$  phase lattice parameters calculated by DFT and obtained with Le Bail refinements on sample Ni21.5 to Ni40 diffractograms are plotted in **Fig 13**. The lattice parameters found experimentally at 1000°C are in good agreement with DFT relaxed structure and comprised between the values calculated for 25 at%.Ni and 50 at%.Ni concentrations in  $\text{Co}_3\text{W-DO}_a$ . The experimental lattice parameter evolution with nickel addition does not feature any discernible trend.

x(Ni)	Ordered formation enthalpy (kJ/mol)	SQS superlattice formation enthalpy (kJ/mol)	Number of atoms for SQS calculations	Ni site occupancy on site 2a	Ni site occupancy on site 4e
0.25	-6.587	-5.931	48	0	1/2
0.25	-6.587	-6.536	72	1/3	1/3
0.50	-8.283	-8.740	48	1	1/2
0.50	-8.283	-8.194	72	2/3	2/3

**Table 8.** SQS formation enthalpies for the  $Co_3W-D0_a$  phase with 2b sublattice fully occupied by W.

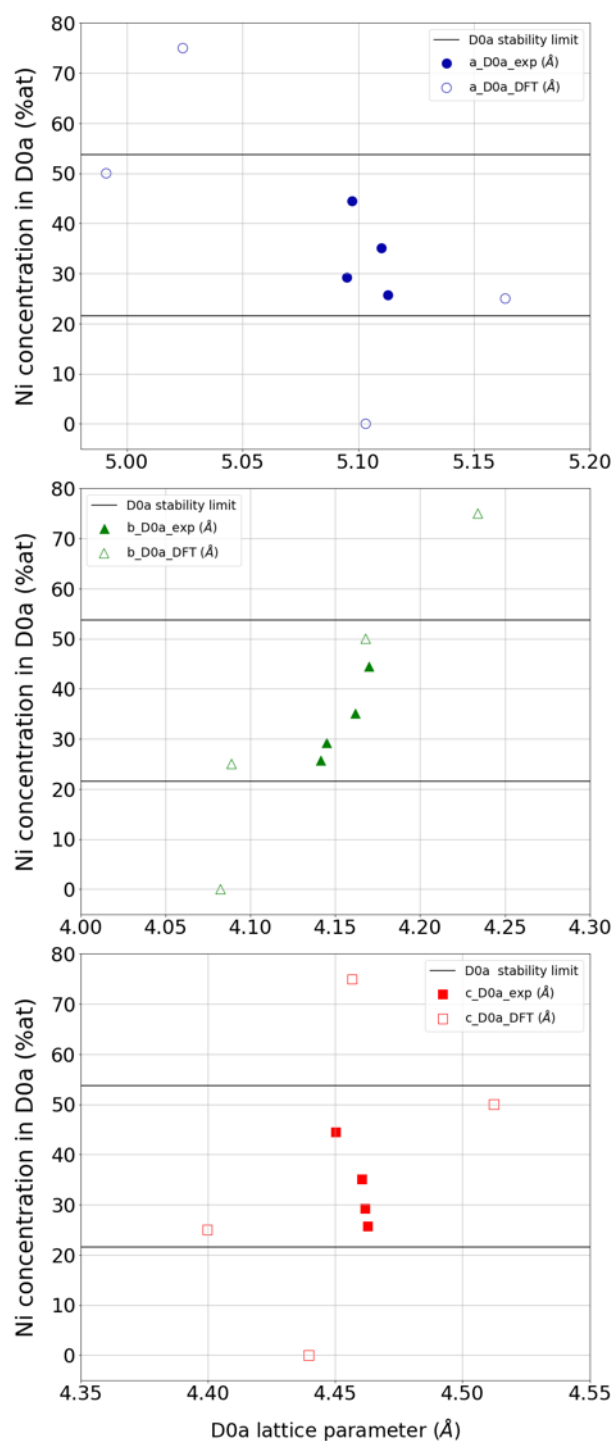


**Fig 13.**  $\text{Co}_3\text{W-D0}_a$  lattice parameter evolution with Ni content as found from DFT calculations and Le Bail refinements on samples equilibrated at 1000°C.

## 5. Conclusions

Samples within the Co–Ni–W system along the 30 at% W isocompositional line were prepared, heat-treated at 800°C and 1000°C and characterized through different methods: X-ray diffraction, electronic diffraction, SEM observations, EPMA composition measurements, TGA-DSC analysis, DFT and SQS calculations. New experimental data were provided to assess phase equilibria evolution as a function of chemical composition and temperature between 800°C and 1000°C.

Zhu *et al.* [14] pointed out the significant Ni solubility of the  $(\text{Co,Ni})_3\text{W}$  like structures at 800°C but could not identify with certainty the phases at equilibrium since they relied on chemical compositions. The intermetallic phase called  $\text{Co}_3\text{W-D0}_a$  was found stable over a wide composition range in Ni (52.49 at% at 1000°C and more than 58.68 at% at 800°C) and the transition from  $\text{Co}_3\text{W-D0}_{19}$  to  $\text{Co}_3\text{W-D0}_a$  with nickel addition was studied in terms of temperature and composition. Further experiments are necessary to better understand the phase transition between  $\text{Co}_3\text{W-D0}_{19}$  to  $\text{Co}_3\text{W-D0}_a$  which is located around 30 at% Ni at 800°C and around 25 at% Ni at 1000°C.

Besides the presence of several ternary phase domains were established including  $\text{BCC\_A2+Co}_3\text{W-D0}_a+\text{Co}_7\text{W}_6-\mu$  and  $\text{BCC\_A2+Co}_3\text{W-D0}_a+\text{FCC\_A1}$  and assumptions on phase domain evolution with temperature were put forward based on all the obtained experimental results. The obtained results emphasize the lacks of the previous thermodynamic descriptions for the Co–Ni–W system at temperatures lower than 1300°C. Therefore, there is a conspicuous need for a revamped CALPHAD model. Thermodynamic data extracted from DFT calculations are consistent with experimental results and will help to establish a better description of intermetallic phases involved in the Co–Ni–W system. More experimental investigations are being conducted to achieve a better understanding of phase equilibria over a wide range of compositions and temperatures and a CALPHAD optimization of the ternary Co–Ni–W system is ongoing.

## Acknowledgements

This work was supported and financed by Plansee Tungsten Alloys and l'Agence de l'innovation de défense (AID) within the framework of Nicolas Bouliez's PhD thesis.

The assistance of Jean-Marc Bigot (Plansee Tungsten Alloys), Ruben Vera from “Centre de Diffraction Henri Longchambon” (CDHL, <http://cdalpha.univ-lyon1.fr/index.php>) for XRD measurements and the members of the « Centre Technologique des Microstructures, Université Lyon 1 » (CT $\mu$ , <http://microscopies.univ-lyon1.fr>) for SEM characterizations are gratefully acknowledged.

The assistance and granted access to calculation means by the Pôle Scientifique de Modélisation Numérique (ENS-LYON) has been very valuable for the achievement of this work.

Calculations were performed using HPC resources from GENCI-CINES (096175) and supercomputer at IMR, Tohoku University (20S0513).

Finally, the authors wish to thank the GDR CNRS n°3584 (TherMatTH) community where fruitful discussions led to collaboration on this project.

## References

- [1] A. Harte, M. Atkinson, A. Smith, C. Drouven, S. Zaefferer, J. Quinta da Fonseca, M. Preuss, The effect of solid solution and gamma prime on the deformation modes in Ni-based superalloys, *Acta Materialia*. 194 (2020) 257–275.
- [2] A. Nowotnik, Nickel-based Superalloys, Reference Module in Materials Science and Materials Engineering. (2016).
- [3] O. Rapaud, J.-M. Joubert, Modelisation thermodynamique par la méthode CALPHAD, GDR CNRS 3584 TherMatHT Thermodynamic Des Matériaux à Haute Température. (n.d.). <https://www.thermatht.fr/modelisation-thermodynamique-par-la-methode-calphad/> (accessed October 13, 2020).
- [4] P. Gustafson, A. Gabriel, I. Ansara, A thermodynamic evaluation of the C-Ni-W system, *Z Metallkde.* (1986) 639–647.
- [5] I. Isomäki, M. Hämäläinen, M. Braga, M. Gasik, First principles, thermal stability and thermodynamic assessment of the binary Ni-W system, *Int. J. Mater. Res.* (2017) 1025–1035.
- [6] A.F. Guillermet, Thermodynamic properties of the Co-W-C system, *Metallurgical Transactions A*. 20A (1989) 935–956.
- [7] A. Markström, B. Sundman, K. Frisk, A revised thermodynamic description of the Co-W-C system, *Journal of Phase Equilibria and Diffusion*. 26 (2005) 152–160.
- [8] J. Sato, K. Oikawa, R. Kainuma, K. Ishida, Experimental verification of magnetically induced phase separation in  $\alpha$ Co phase and thermodynamic calculations of phase equilibria in the Co-W system, *Material Transactions*. 46 (2005) 1197–1207.
- [9] B. Kaplan, A. Blomqvist, M. Selleby, S. Norgren, Thermodynamic analysis of the W-Co-Cr system supported by ab initio calculations and verified with quaternary data., *CALPHAD*. 50 (2015) 59–67.
- [10] B. Kaplan, An updated thermodynamic description of the W-Co and W-Co-Cr systems with focus on ground state intermetallic phases, *CALPHAD*. 66 (2019) 1–6.
- [11] P. Wang, W. Xiong, U.R. Kattner, Thermodynamic re-assessment of the Al-Co-W system, *CALPHAD*. 59 (2017) 112–130.
- [12] A.F. Guillermet, Assessment of the thermodynamic properties of the Ni-Co system, *Z. Metallkde.* 78 (1987) 639–647.
- [13] A.F. Guillermet, Thermodynamic of the Co-Ni-W system : A preliminary CALPHAD analysis, TRITA-MAC. (1988).
- [14] L. Zhu, C. Wei, L. Jiang, Z. Jin, J.-C. Zhao, Experimental determination of the phase diagrams of the Co-Ni-X (X=W,Mo,Nb,Ta) ternary systems using diffusion multiples, *Intermetallics*. 93 (2018) 20–29.
- [15] J.M. Walsh, J. Donachie, On a new intermetallic phase on the nickel-tungsten system, *Metallurgical Transactions*. 4 (1973) 2854–2855.
- [16] H. Hofmann, Konstitution des W-Ni-Fe systems und mechanische eigenschaften W-reicher W-Ni-Fe Legierungen, Technischen Universität Berlin, 1983.
- [17] K. Poulsen, S. Rubaek, E. Langer, A new intermetallic phase in the W-Ni system, *Scripta Metallurgica*. 8 (1974) 1297–1300.
- [18] R. Cury, J.-M. Joubert, S. Tusseau-Nenez, E. Leroy, A. Allavena-Valette, On the existence and the crystal structure of Ni<sub>4</sub>, NiW, NiW<sub>2</sub> compounds, *Intermetallics*. 17 (2009) 174–178.
- [19] S.J.B. Kurz, S.B. Maisel, A. Leineweber, M. Höfler, S. Müller, E.I. Mittemeijer, Discovery of a thermally persistent h.c.p solid-solution phase in the Ni-W system, *Journal of Applied Physics*. 116 (2014) 083515-1 083515-9.
- [20] V. Subrayama Sarma, J. Eickemeyer, C. Mickel, L. Schultz, On the cold rolling textures in some fcc Ni-W alloys, *Material Science and Engineering A*. 380 (2004) 30–33.
- [21] L.A. Neumeier, J.L. Holman, The tungsten-cobalt system for compositions to 85 atomic percent cobalt, United States Department of the Interior, Bureau of Mines, 1967. <https://babel.hathitrust.org/cgi/pt?id=mdp.39015078540864&view=1up&seq=1> (accessed May 7, 2020).
- [22] A. Gabriel, Remplacement du cobalt dans les carbures cémentés, Institut National Polytechnique de Grenoble, 1984.
- [23] J.-M. Joubert, N. Dupin, Mixed site occupancies in the  $\mu$  phase, *Intermetallics*. 12 (2004) 1373–1380.
- [24] G. Östberg, B. Jansson, H.-O. Andrén, On spinodal decomposition in the Co-W system, *Scripta Materialia*. 54 (2006) 595–598.
- [25] Z. Jin, W. Gan, C. Qiu, A study of the isothermal section of the W-Ni-Co system at 1300°C, *Material Science and Engineering*. A124 (1990) 211–213.
- [26] V.S. Shipovskov, L.L. Meshkov, E.M. Sokolovskaya, Phase equilibria in nickel-cobalt-tungsten system, *Vestnik Moskovskogo Universiteta*. 22 (1981) 74–77.
- [27] J.-L. Pouchou, F. Pichoir, Un nouveau modèle de calcul pour la microanalyse quantitative par spectrométrie de rayons X. Partie 1 : Application à l'analyse d'échantillons homogènes, *La Recherche Aérospatiale*. (1984) 167–191.
- [28] J. Rodriguez-Carvajal, FULLPROF : A Program for Rietveld Refinement and Pattern Matching Analysis, in: Toulouse, 1990: p. 127.
- [29] P. Perdew, K. Bürke, M. Ernzerhof, Generalized Gradient Approximation made simple, *Physical Review Letters*. 77 (1996) 3865–3868.

- [30] P.E. Blöchl, Projector augmented-wave method, *Physical Review B*. 50 (1994) 17953–17979.
- [31] J.-C. Crivello, R. Souques, A. Breidi, J.-M. Joubert, ZenGen a tool to generate ordered configurations for systematic first principle calculations : The Cr--Mo--Ni--Re system as a case study, *CALPHAD*. 51 (n.d.) 233–240.
- [32] A. Zunger, S.-H. Wei, L.G. Ferreira, James.E. Bernard, Special Quasirandom Structures, *Physical Review Letters*. 65 (1990) 353–356.
- [33] A. van de Walle, P. Tiwary, M. de Jong, D.L. Olmsted, M. Asta, A. Dick, D. Shin, Y. Wang, L.-Q. Chen, Z.-K. Liu, Efficient stochastic generation of special quasirandom structures, *CALPHAD*. 42 (2013) 13–18.